ISSN 1063-7737, Astronomy Letters, 2016, Vol. 42, No. 8, pp. 531–543. © Pleiades Publishing, Inc., 2016.
Original Russian Text © P.A. Gritsyk, B.V. Somov, 2016, published in Pis'ma v Astronomicheskii Zhurnal, 2016, Vol. 42, No. 8, pp. 586–599.

X-ray and Microwave Emissions from the July 19, 2012 Solar Flare: Highly Accurate Observations and Kinetic Models

P. A. Gritsyk* **and B. V. Somov****

Sternberg Astronomical Institute, Universitetskii pr. 13, Moscow, 119992 Russia

Received February 10, 2016

Abstract—The M7.7 solar flare of July 19, 2012, at 05:58 UT was observed with high spatial, temporal, and spectral resolutions in the hard X-ray and optical ranges. The flare occurred at the solar limb, which allowed us to see the relative positions of the coronal and chromospheric X-ray sources and to determine their spectra. To explain the observations of the coronal source and the chromospheric one unocculted by the solar limb, we apply an accurate analytical model for the kinetic behavior of accelerated electrons in a flare. We interpret the chromospheric hard X-ray source in the thick-target approximation with a reverse current and the coronal one in the thin-target approximation. Our estimates of the slopes of the hard X-ray spectra for both sources are consistent with the observations. However, the calculated intensity of the coronal source is lower than the observed one by several times. Allowance for the acceleration of fast electrons in a collapsing magnetic trap has enabled us to remove this contradiction. As a result of our modeling, we have estimated the flux density of the energy transferred by electrons with energies above 15 keV to be $\sim 5 \times 10^{10}$ erg cm^{-2} s^{-1}, which exceeds the values typical of the thick-target model without a reverse current by a factor of $\sim$5. To independently test the model, we have calculated the microwave spectrum in the range 1–50 GHz that corresponds to the available radio observations.

DOI: 10.1134/S1063773716080016

Keywords: *Sun, flares, accelerated electrons, reverse current, bremsstrahlung, gyrosynchrotron emission, coronal source.*

1. INTRODUCTION

According to the fundamental theoretical views of the solar flare mechanism (Giovanelli 1948; Parker 1957; Sweet 1958, 1969; Syrovatskii 1962, 1966), strong magnetic fields in the solar atmosphere, whose energy is converted into the kinetic energy of charged particles and magnetohydrodynamic (MHD) plasma flows through magnetic reconnection, are the flare energy source. Despite the great variety of physical conditions under which this mechanism of primary energy release in solar flares is realized, the overall picture of the flare and its scenario are currently believed to be understandable and well known (see, e.g., Priest and Forbes 2000; Somov 2013). Conditions for fast magnetic reconnection are formed in the solar corona before the beginning of the impulsive phase. A huge amount of energy is released during the impulsive phase (from several seconds to several minutes). During reconnection, the electrons, protons, and other ions are accelerated by an electric field to energies much higher than the thermal energies of particles in the solar corona and chromosphere (Hudson and Ryan 1995; Somov 2000; Aschwanden 2002; Miroshnichenko 2015).

The electrons, whose mass is much smaller than that of the protons, easily acquire high velocities, run away from the acceleration region, a reconnecting current layer, and rapidly propagate along reconnected magnetic field lines. In this case, the density of the background plasma, i.e., the plasma in the fast particle propagation path, changes from $\sim 10^9$ cm^{-3} in the corona to $\sim 10^{11}$ cm^{-3} or higher in the chromosphere (Caspi et al. 2014). Because of the low background plasma density, the accelerated electrons traverse the coronal segment of the flare loops formed by reconnected field lines almost without Coulomb energy losses, producing hard X-ray bremsstrahlung in the corona. Penetrating into the chromosphere, where the plasma density is much higher than that in the corona, the accelerated electrons rapidly lose their kinetic energy through Coulomb collisions, also generating hard X-ray emission (Syrovatskii and Shmeleva 1973; Somov and Syrovatskii 1976).

A typical picture of a flare is schematically shown in Fig. 1. The reconnected magnetic field lines **B**

*E-mail: pgritsyk@gmail.com
**E-mail: somov.boris@gmail.com

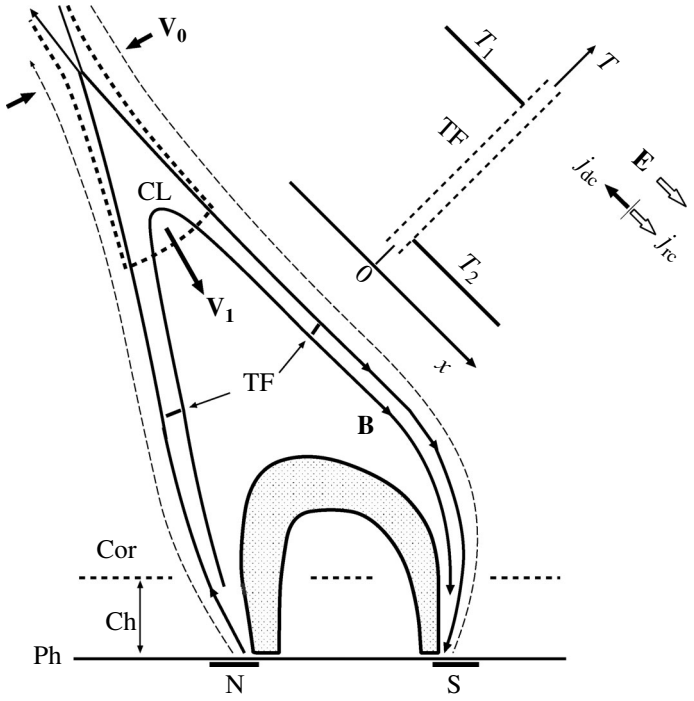

Fig. 1. General formulation of the problem of electrons accelerated in a reconnecting current layer (CL) that run away from a hot plasma with temperature T_1 through a turbulent front (TF) into a colder target plasma with temperature T_2.

move from the current layer (CL) with velocity $\mathbf{V}_1$ downward, toward the chromosphere (Ch) and the photosphere (Ph); N and S are a pair of photospheric magnetic field sources, for example, sunspots.

To check whether the kinetic description of solar flares proposed below is correct, we consider the July 19, 2012 flare that was observed with a high spatial resolution in various regions of the electromagnetic spectrum. This flare is of particular interest for modeling, because it was at the solar limb, while the flare loop was located in the plane of the sky. The chromospheric hard X-ray and optical sources and the coronal X-ray source are clearly seen in the images taken onboard the RHESSI and SDO spacecraft (Krucker and Battaglia 2014). In addition, there is a microwave spectrum (Liu 2013).

The classical thick-target (Syrovatskii and Shmeleva 1972) and thin-target (for a review, see Somov and Syrovatskii 1976) models are currently widely used to interpret the hard X-ray observations. Nevertheless, these models experience considerable difficulties in describing powerful solar flares (Gritsyk and Somov 2014), because they disregard the reverse current that compensates the electric current of accelerated electrons (Diakonov and Somov 1988; Litvinenko and Somov 1991). A fundamental peculiarity of the mentioned thick-target models with a reverse current is that they are two-dimensional in velocity space (see Somov 2012, Chapter 4). This enables the accelerated electrons to reverse the direction of their propagation almost without Coulomb energy losses. As a consequence, harder (compared to the models without a reverse current) injection spectra of accelerated electrons are needed to provide a sufficient electron flux density in the emission source, which determines the observed spectral slopes of the chromospheric and coronal hard X-ray sources. For example, for the July 19, 2012 solar flare, the slopes of the observed spectra for the emission sources in the corona and chromosphere cannot be explained in terms of the classical models without a reverse current.

The ratio of the intensities of the chromospheric and coronal hard X-ray sources, their temporal and spectral peculiarities also depend on how efficiently the betatron heating and first-order Fermi acceleration operate inside the flare loops, which act as collapsing magnetic traps (Somov and Kosugi 1997). Bogachev and Somov (2007) showed that both effects related to the acceleration of electrons in a trap should be taken into account to explain the observed intensity of the coronal X-ray sources.

The goal of this paper is to interpret the observations of the July 19, 2012 flare in terms of the model

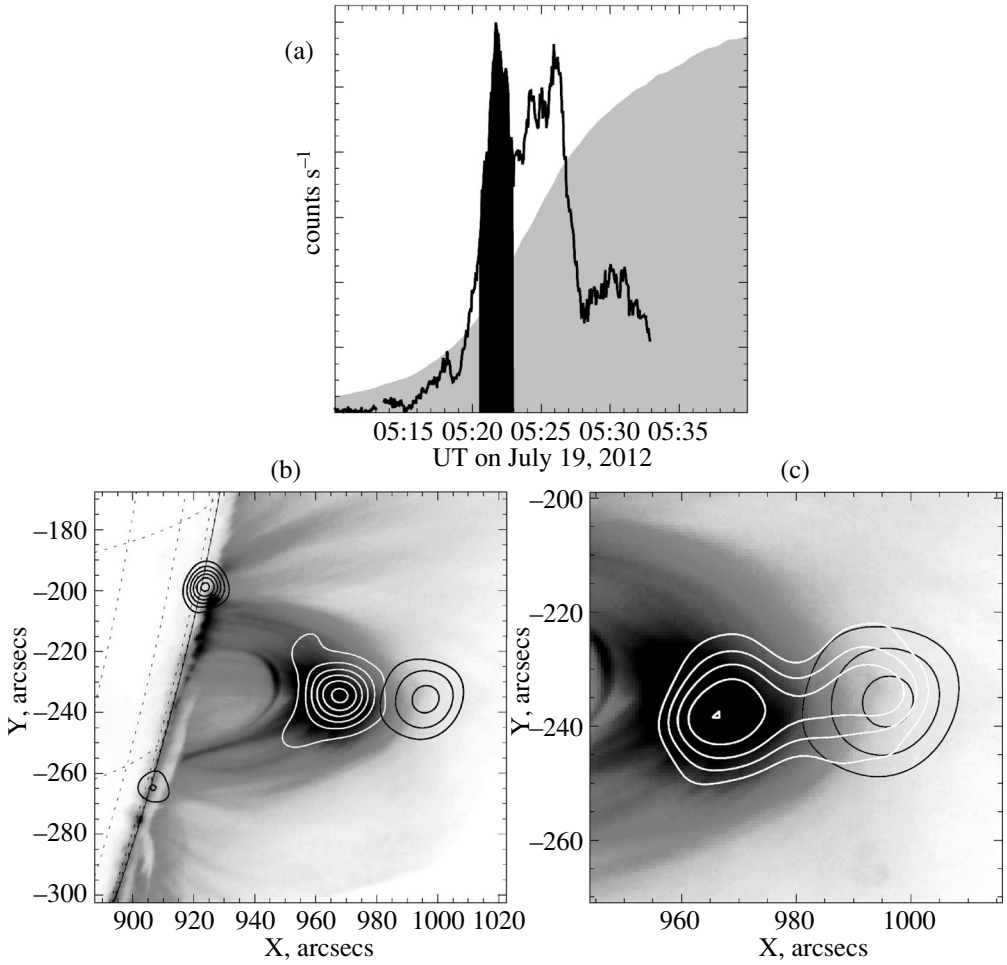

Fig. 2. Observations of the July 19, 2012 flare. (a) The time profile (black curve) of the hard X-ray (30–80 keV) emission from the entire flare based on RHESSI data. The dark vertical band is the time interval of data accumulation for imaging. The gray background indicates the profiles of the soft X-ray emission based on GOES data. (b, c) SDO/AIA images at a wavelength of 193 Å: (b) the flare loop with the coronal and chromospheric sources, (c) the coronal source. The black contours indicate the levels of hard X-ray (30–80 keV) emission based on RHESSI data. The white contours indicate the levels of X-ray emission in the 6–8 (b) and 16–18 keV (c) bands.

with a reverse current. We are going to describe the coronal X-ray source in terms of the thin-target model by taking into account the acceleration of electrons in a collapsing magnetic trap and the chromospheric one in terms of the thick-target model with a reverse current. The observational data on the flare are presented in Section 2. The kinetic model that is used to explain the observed emission characteristics in the flare is presented in Section 3. The calculated X-ray spectra and their comparison with the observed ones are presented in Section 4. The electron beam parameters and the plasma heating power in the chromosphere are given in Section 5. The discussion of our results and conclusions are contained in the last section of the paper.

2. OBSERVATIONS OF THE JULY 19, 2012 FLARE

The M7.7 solar flare was observed on July 19, 2012, onboard the Ramaty High-Energy Solar Spectroscopic Imager (RHESSI, Lin et al. 2002) and Solar Dynamics Observatory (SDO, Lemen et al. 2012) satellites with a high spatial resolution as well onboard the Geostationary Operational Environmental Satellite (GOES) satellite and at the Nobeyama Radio Observatory using the NoRP and NoRH instruments. Since the flare was located at the solar limb, the X-ray sources are clearly seen (Fig. 2): the coronal one above the flare loop and two chromospheric sources at the loop footpoints; the flare loops were also observed in the optical and microwave

ranges (Liu et al. 2013; Liu 2013; Krucker and Battaglia 2014).

The observational data in the hard X-ray range used here were obtained by adding the results of individual measurements in the time interval indicated by the dark band on the upper panel of Fig. 2 (Krucker and Battaglia 2014). The band center coincides with the maximum of the first, highest hard X-ray burst at time 05:22:30 UT. Obviously, the chosen interval corresponds to the greatest power of energy release in the form of accelerated electrons during the impulsive flare phase. The greatest number of energetic electrons per unit time emerge from the acceleration source and generate the most powerful hard X-ray flux (Krucker et al. 2015).

Consider in more detail the observed picture of the flare. One coronal and two chromospheric sources were observed in the hard X-ray range (Figs. 2b, 2c). The southern chromospheric source is very weak, because it is partially behind the limb. High-quality X-ray observations are available for the northern chromospheric source; it was chosen for our modeling in the thick-target approximation with a reverse current. The coronal source was above the flare loop, was observed with a high resolution, and was chosen for the description in the thin-target approximation.

The input parameters of the kinetic model considered in Section 3 can be estimated from the observations of the coronal hard X-ray source, which we think to be located in the immediate vicinity of the electron acceleration region, a high-temperature reconnecting current layer. According to the estimates by Krucker and Battaglia (2014), the angular size of the source is $15''$. The lower boundary of the energy spectrum of accelerated electrons is $\mathcal{E}_{\min 1} \approx 15$ keV. As a rule, this quantity is estimated with a large error due to the superposition of thermal and nonthermal injection spectra characteristic of any flare (see, e.g., Somov and Syrovatskii 1976). This fact introduces considerable inaccuracies into the determination of the hard X-ray intensity, but it barely affects the estimate of its spectral slope at sufficiently high energies, where the X-ray bremsstrahlung is definitely nonthermal.

The duration of the first (and largest) hard X-ray peak being considered here is $\approx$100 s, which is definitely much greater than even the rough estimates of the characteristic time scales for Coulomb collisions between accelerated electrons and plasma electrons in the target. This allows us to use the stationary approximation, to be more precise, the approximation of continuous injection of accelerated electrons into the target when constructing the kinetic model in Section 3 (see Somov and Syrovatskii 1976).

In this paper, the spectrum of nonthermal electrons is arbitrarily divided into two parts, each of which is described in terms of the corresponding kinetic model. The evolution of the electron spectrum with the boundaries $\mathcal{E}_{\min 1} = 15$ keV and $\mathcal{E}_{\max 1} = 120$ keV is described in the approximation of the model with a reverse current (Gritsyk and Somov 2014). It is convenient to use the classical model of Leach and Petrosian (1981) to describe the propagation of electrons with even higher energies, from $\mathcal{E}_{\min 2} = 120$ keV to $\mathcal{E}_{\max 2} = 1200$ keV, because such particles barely lose their energy through Coulomb collisions and in the reverse-current electric field and contribute insignificantly to the intensity of the observed X-ray emission. Nevertheless, these electrons (Holt and Ramaty 1969) contribute significantly to the high-frequency part of the gyrosynchrotron radio spectrum, which we calculate to additionally test the model.

Here, we give the estimates of various parameters for the July 19, 2012 flare from Krucker and Battaglia (2014) that are important for the subsequent discussion. The temperature of the "cold" target plasma behind the turbulent front TF (Fig. 1) is high, $T_2 \approx 21$ MK. The temperature of the source of accelerated electrons, i.e., the super-hot plasma, is not known from observations and is taken to be $T_1 \approx 100$ MK, i.e., it is estimated in order of magnitude based on the theory of super-hot turbulent current layers (Chapter 8 in Somov (2013)). The plasma number density in the region where the coronal source is located is $n_2 \approx 3 \times 10^9$ cm^{-3} (see Fig. 8.8 in Somov (2013)). The magnetic field strength at the loop top is $B_0 \sim 10^2$ G.

As has been noted above, in the flare under consideration we analyze two hard X-ray sources: the coronal and northern chromospheric ones. The coronal source has a spectral slope $\varphi = 4.6 \pm 0.2$ with a flux of 0.1 photons cm^{-2} keV^{-1} at a photon energy of 50 keV, while the chromospheric one has $\varphi = 3.0 \pm 0.2$ with a flux of 1 photon cm^{-2} keV^{-1}. The microwave spectrum was taken at the NoRP instrument with a high temporal resolution. From Liu (2013) we took the data on this spectrum at the time of maximum in the X-ray range, i.e., at 05:22:30 UT. Below, we present the proposed kinetic flare model, the modeling results, and their comparison with the observations.

3. KINETIC FLARE MODEL

3.1. Allowance for the Reverse-Current Effect

The first self-consistent analytical models (Diakonov and Somov 1988; Litvinenko and Somov 1991) in which the necessity of allowance for the

reverse-current effect was proven have been improved and applied to the description of new highly accurate space observations (Gritsyk and Somov 2014). In this section, we consider the analytical model that is used to describe the propagation of electrons accelerated in the July 19, 2012 flare. Below, we provide the main model assumptions, the analytical solution for the distribution function, and the model parameters.

In the schematic Fig. 1, the coronal part of the flare can be divided into two parts: the electron acceleration region near a reconnecting current layer with temperature T_1 and the region of a colder plasma with temperature T_2. A thin turbulent front TF, the boundary below which the corresponding kinetic problem is solved, is formed between these two regions. We will assume that the magnetic field is uniform and perpendicular to the turbulent front. The condition for the distribution function at the boundary TF is

$$f_{\mathbf{v}ff}(v,\theta,0) = f_{\mathbf{v}s}(v,\theta)\Theta(v-v_{\min})\Theta(v_{\max}-v), \quad (1)$$

where v is the velocity of the electrons, θ is the angle between the velocity vector $\mathbf{v}$ and the magnetic field direction, $v_{\min}$ and $v_{\max}$ are the minimum and maximum velocities of the electrons in the beam, the theta-function $\Theta(x)=1$ at $x\geq 0$ and $\Theta(x)=0$ at $x<0$. Here and below, the subscript $\mathbf{v}$ indicates that $f_{\mathbf{v}}$ is the particle velocity vector distribution function.

It is convenient to normalize the distribution function to the flux density of the energy transferred by flare-accelerated electrons:

$$F = \int f_{\mathbf{v}}(v,\theta,0) \times v\cos\theta\frac{m_e v^2}{2}d^3\mathbf{v},\ \mathrm{erg\ cm^{-2}\ s^{-1}}, \quad (2)$$

where m_e is the electron mass. When modeling the flare, the parameter (2) is chosen in such a way that the calculated intensity of the X-ray emission from the chromospheric source corresponds to the observed one.

The forward-flying accelerated electrons produce an electric current that we will call the direct one. Given the sign of the electron charge, the direct current is directed toward the turbulent front TF (Fig. 1). The reverse current is produced by the thermal electrons of the cold plasma inside the target moving under the action of the reverse-current electric field, which can be found from Ohm's law. The assumption that the direct current is balanced by the reverse current is significant but justified here. It means that the very rapid reverse-current generation process (Van den Oord 1990) manages to balance the direct current in a time comparable to the period of plasma oscillations, which is much shorter than the Coulomb collision time in the conditions we consider.

We describe the behavior of the distribution function of accelerated electrons in the target by the kinetic equation (see Section 4.5.2 in Somov (2012))

$$v\cos\theta\frac{\partial f_{\mathbf{v}}}{\partial l} - \frac{eE}{m_e}\cos\theta\frac{\partial f_{\mathbf{v}}}{\partial v} - \frac{eE}{m_e v}\sin^2\theta\frac{\partial f_{\mathbf{v}}}{\partial\cos\theta} = St_{\mathrm{L}}(f_{\mathbf{v}}),$$

where l is the particle penetration depth into the target, e is the electron charge, and E is the reverse-current electric field strength. Here, we take into account the fact that on time scales of the order of the Coulomb collision time in the cold target plasma, we may consider the injection of electrons as a stationary process and their distribution in the target as a steady-state one (the derivative $\partial/\partial t$ is zero). The right-hand side of the equation contains a linearized Landau collision integral.

In dimensionless variables, the kinetic equation is (Gritsyk and Somov 2011):

$$\mu z^2\frac{\partial f_{\mathbf{v}}}{\partial s} - 2\varepsilon\mu z^2\frac{\partial f_{\mathbf{v}}}{\partial z} - \varepsilon z\left(1-\mu^2\right)\frac{\partial f_{\mathbf{v}}}{\partial\mu} = z\frac{\partial f_{\mathbf{v}}}{\partial z} + \tau z\frac{\partial^2 f_{\mathbf{v}}}{\partial z^2} + \frac{1}{2}\frac{\partial}{\partial\mu}\left[(1-\mu^2)\frac{\partial f_{\mathbf{v}}}{\partial\mu}\right], \quad (3)$$

where z is the dimensionless energy of the accelerated electrons, μ is the dimensionless angle, s is the dimensionless electron penetration depth into the target, and ε is the dimensionless electric field strength.

The distribution function $f_{\mathbf{v}s}$ of electrons in the source, in a reconnecting super-hot turbulent current layer, consists of two parts: the thermal and nonthermal ones. The first is usually taken in Maxwellian form (Diakonov and Somov 1988); the second is taken in the form of a power law (Litvinenko and Somov 1991). We will consider the fast nonthermal electrons. Therefore, as a boundary condition we will take only the part of the distribution function of electrons in their source (see (1)) in the form of a power law:

$$f_{\mathbf{v}}(z,\mu,0) = K_0 z^{-\gamma_{\mathbf{v}}}\Theta(z-z_{\min})\Theta(z_{\max}-z). \quad (4)$$

Here, the dimensionless energies $z_{\min}$ and $z_{\max}$ correspond to the lower and upper boundaries of the energy spectrum of accelerated electrons. The constant K_0 is determined from the normalization condition (2) and, given condition (4), is

$$K_0 = \begin{cases} F\,(3-\gamma_{\mathbf{v}})/\left[\left(2\pi(k_{\rm B}T_1)^3/{m_e}^2\right)\left({z_{\rm max}}^{3-\gamma_{\mathbf{v}}} - {z_{\rm min}}^{3-\gamma_{\mathbf{v}}}\right)\right], & \gamma_{\mathbf{v}} \neq 3, \\ F/\left[\left(2\pi(k_{\rm B}T_1)^3/{m_e}^2\right)\ln\left(z_{\rm max}/z_{\rm min}\right)\right], & \gamma_{\mathbf{v}} = 3. \end{cases}$$

Previously (Gritsyk and Somov 2011), we found a general solution of Eq. (3):

$$f_{\mathbf{v}}(z,\mu,\phi) = K_0 \times \left[z + 2\phi + \frac{1}{2\varepsilon(x)}\left(\ln\frac{1+Y}{1-Y} - \ln\frac{1+\mu}{1-\mu}\right)\right]^{-\gamma_{\mathbf{v}}}, \quad (5)$$

where

$$Y = {\rm sgn}\mu\left(\mu^2 + 2\phi/z\right)^{1/2}(1+2\phi/z)^{-1/2}.$$

The function ${\rm sgn}\mu = -1$ at $\mu < 0$ and ${\rm sgn}\mu = +1$ at $\mu \geq 0$, the dimensionless potential of the reverse-current electric field

$$\phi = \int_0^s \varepsilon(s')ds',$$

the dimensionless electric field

$$\varepsilon(x) = \begin{cases} \varepsilon(\phi), & \mu \geq 0, \\ \varepsilon(z\mu^2/2), & \mu < 0, \end{cases}$$

the function

$$\varepsilon(\phi) = \begin{cases} [2abK_0/(\gamma_{\mathbf{v}}-1)]^{1/2}(2\phi_0)^{(1-\gamma_{\mathbf{v}})/2} = \varepsilon_0 = {\rm const}, & \phi < \phi_0 = z_{\rm cr}/2, \\ [2abK_0/(\gamma_{\mathbf{v}}-1)]^{1/2}(2\phi)^{(1-\gamma_{\mathbf{v}})/2}, & \phi > \phi_0, \end{cases} \quad (6)$$

the parameters $a = \pi e(2k_{\rm B}T_1/m_e)^2$ and $b = k_{\rm B}T_1/(2\pi e^3 n_2 \sigma \ln\Lambda)$.

The model allows the distribution function of accelerated electrons in the solar corona and chromosphere to be estimated at various depths. The kinetic equation (3) under the specified boundary condition (4) uniquely determines the evolution of the beam of accelerated particles in the target (see Eq. (5)) and the characteristics of the hard X-ray and microwave emissions generated by them. In Section 2, we presented the parameters near the turbulent front TF (Fig. 1) used to model the July 19, 2012 flare: the hot and cold plasma temperatures T_1 and T_2 and the cold plasma number density n_2. Before we turn to modeling the flare, let us discuss several additions to the kinetic model described above.

When calculating the hard X-ray emission of accelerated electrons in specific solar flares, Syrovatskii and Shmeleva (1972) arbitrarily assumed the upper boundary of the electron energy spectrum to be infinitely large. This is quite justifiable. Even for powerful flares with a very hard injection spectrum, the slope $\gamma_{\mathbf{v}} \gtrsim 2$. Therefore, the estimates of the radiation flux density barely change with chosen upper boundary of the spectrum (see also Gritsyk and Somov 2014).

We will assume that the evolution of the distribution function of accelerated electrons with energies below some arbitrary value z_p corresponding to the dimensional energy of 120 keV (see Section 2) is defined by the solution (5). It describes well the distribution function at both small ($s \sim 0$, the thin-target approximation) and large ($s \to \infty$, the thick-target approximation with a reverse current) target thicknesses.

For the case where the energy of the accelerated electrons $z > z_p$, by neglecting the Coulomb collisions and the weak influence of the reverse-current electric field on the beam electrons, Leach and Petrosian (1981) obtained an analytical solution of the simple kinetic equation (cf. (3)) that takes into account only the magnetic field nonuniformity:

$$\frac{\partial f_{\mathbf{v}}}{\partial s} = \frac{1-\mu^2}{2}\alpha_B\frac{\partial f_{\mathbf{v}}}{\partial \mu}, \quad (7)$$

where

$$f_{\mathbf{v}}(z,\mu,s) = f_{\mathbf{v}0}\left(z, (1-(1-\mu^2)e^{\alpha_B})^{1/2}\right), \quad (8)$$

$\alpha_B = \ln(B(s)/B(0))$ is the logarithm of the ratio of the magnetic field at the footpoints of the flare loop to the field at its top. Thus, using the analytical solutions (5) and (8), we can obtain a model description of the propagation of an electron beam in the solar atmosphere for both $z \leq z_p$ and $z > z_p$, respectively.

3.2. Allowance for the Acceleration of Electrons in a Magnetic Trap

Yet another significant physical effect must supplement the kinetic description (3)–(8). Bogachev and Somov (2007) considered the betatron and Fermi acceleration of electrons in a collapsing magnetic trap and showed that both mechanisms could affect significantly the particle energy spectrum. An interesting feature of the acceleration in collapsing magnetic traps is that an initially power-law injection spectrum remains a power-law one after the acceleration, shifting toward higher energies. This shift depends on the trap contraction parameters and the mirror ratio, which can be estimated from observations. It is well known that the impulsive flare phase can reach several minutes in which the flare loops, which are magnetic traps, change noticeably their sizes. Indeed, the characteristic velocity of the plasma and the magnetic field lines frozen into it is $\sim 10^3$ km s^{-1}. Consequently, the acceleration of electrons in a collapsing magnetic trap should be taken into account when modeling a solar flare (see Somov and Kosugi 1997; Somov and Bogachev 2003).

4. INTERPRETATION OF THE EMISSION SPECTRA

4.1. Hard X-ray Spectrum

We will calculate the hard X-ray spectra of the coronal and chromospheric sources using the analytical solution (5) with the boundary condition (4) for electrons with energies from 15 to 120 keV and the microwave spectrum using the solution (8) with the boundary condition (4) for electrons with energies from 120 to 1200 keV.

For the electron distribution function (5), the hard X-ray emission parameters are calculated as follows. Let $\mathcal{E}_\nu = h\nu/k_{\rm B}T_1$ be the dimensionless photon energy and ϑ be the angle between the wave vector $\mathbf{k}$ and the electron velocity $\mathbf{v}$. We will use the well-known formulas (Elwert and Haug 1970) for the differential cross sections for the bremsstrahlung of X-ray photons polarized parallel and perpendicular to the $(\mathbf{v},\mathbf{k})$ plane,

$$\frac{\partial^2\sigma_{||}}{\partial\Omega\partial(h\nu)} = C\left(A + B\sin^2\vartheta\right)\sigma_0,$$

$$\frac{\partial^2\sigma_{\perp}}{\partial\Omega\partial(h\nu)} = CA\sigma_0.$$

Here,

$$A = \frac{z-\mathcal{E}_\nu/2}{\sqrt{z(z-\mathcal{E}_\nu)}}\ln\frac{\sqrt{z}+\sqrt{z-\mathcal{E}_\nu}}{\sqrt{z}-\sqrt{z-\mathcal{E}_\nu}} - 1,$$

$$B = \frac{(3/2)\mathcal{E}_\nu - z}{\sqrt{z(z-\mathcal{E}_\nu)}}\ln\frac{\sqrt{z}+\sqrt{z-\mathcal{E}_\nu}}{\sqrt{z}-\sqrt{z-\mathcal{E}_\nu}} + 3,$$

$$C = \frac{1}{z\mathcal{E}_\nu}\frac{1-\exp\left(-2\pi\alpha c\sqrt{m_e/2zk_{\rm B}T_1}\right)}{1-\exp\left(-2\pi\alpha c\sqrt{m_e/2(z-\mathcal{E}_\nu)k_{\rm B}T_1}\right)},$$

$$\sigma_0 = \frac{\alpha}{2\pi}\frac{m_ec^2}{k_{\rm B}T_1}\frac{{r^2}_0}{k_{\rm B}T_1},$$

$\alpha = e^2/\hbar c$ is the fine-structure constant, $r_0 = e^2/m_ec^2$ is the classical electron radius.

Let $I_{HXR||}$ and $I_{HXR\perp}$ be the X-ray fluxes at distance R from a given source on the Sun with polarization parallel and perpendicular to the plane formed by the line of sight and the magnetic field lines of the flare loop. The total X-ray flux is then (Nocera et al. 1985)

$$I_{HXR} = I_{HXR\perp} + I_{HXR||} \tag{9}$$

$$= I_{HXR0}\left\{8\int\limits_{\mathcal{E}_\nu}^{\infty} AC\left(\int\limits_0^{\infty} L_0 d\xi\right) zdz\right.$$

$$+\frac{8}{3}\int\limits_{\mathcal{E}_\nu}^{\infty} BC\left(\int\limits_0^{\infty} L_0 d\xi\right) zdz$$

$$\left.+\frac{12\sin^2\psi - 8}{15}\int\limits_{\mathcal{E}_\nu}^{\infty} BC\left(\int\limits_0^{\infty} L_2 d\xi\right) zdz\right\}.$$

Here, ψ is the angle between the line of sight (the direction from the emission source to the observer) and the direction perpendicular to the magnetic field; $L_0 = L_0(z,\phi)$ and $L_2 = L_2(z,\phi)$ are the coefficients of the Legendre polynomial expansion of the distribution function (5). The integration in Eq. (9) is over the plasma column depth

$$\xi = \int\limits_0^l n_2(l')dl',\ {\rm cm}^{-2}.$$

This allows us to avoid the superfluous assumptions about the plasma density distribution in the target and the extent of the X-ray source. The upper limit of integration over the column depth is infinite for a thick target and a specified value for a thin target (Somov and Syrovatskii 1976). As was noted in Section 3.2, the limit of integration over the dimensionless energy z in (9) is assumed to be infinite. The quantity

$$I_{HXR0} = \frac{\alpha}{\pi}\left(\frac{r_0}{R}\right)^2$$

$$\times\, mc^2\frac{KS_{HXR}}{m^2},\ \text{photons keV}^{-1}\ \text{s}^{-1},$$

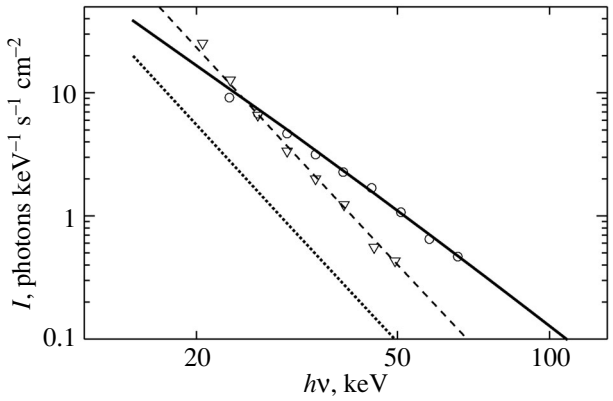

Fig. 3. Observed and calculated hard X-ray spectra for the July 19, 2012 flare. The results of modeling the chromospheric source are represented by the solid straight line; the observations are indicated by the circles. The results of modeling the coronal source without and with allowance made for the acceleration of electrons in a collapsing magnetic trap are represented by the dotted straight line and dashed line, respectively; the observations are indicated by the triangles.

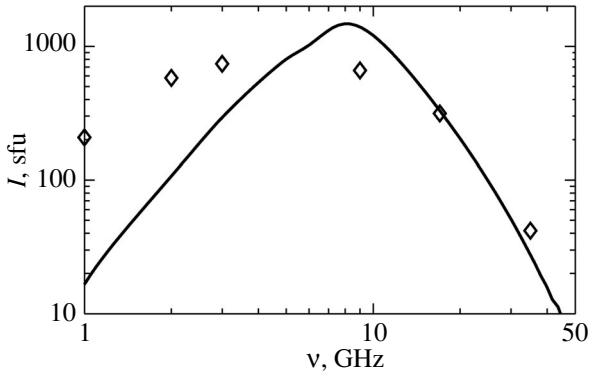

Fig. 4. Microwave spectrum for the July 19, 2012 flare. The modeling results are represented by the solid line; the observations with the NoRP instrument are indicated by the diamonds.

where S_{HXR} is the area of the emission source.

The calculated hard X-ray spectra for the coronal and chromospheric sources are presented in Fig. 3. The observed spectrum for the northern chromospheric source (circles) is reproduced with a high accuracy in the thick-target approximation with a reverse current (solid straight line). This suggests that the model is well applicable and that such parameters of the electron injection spectrum as the energy flux density and the slope were chosen properly.

However, the observed spectrum for the coronal source (triangles) in the thin-target approximation is described poorly. The calculated spectrum (dotted straight line) turned out to be shifted considerably toward lower energies at the correct slope, i.e., coincident with the observed slope of the hard X-ray spectrum.

It seems obvious to us that this shift is related to the additional acceleration of electrons that they acquire being captured into a collapsing magnetic trap (Somov and Kosugi 1997). Electrons with any spectrum (including the Maxwellian one) acquire a kinetic energy in a collapsing magnetic trap through the betatron and Fermi acceleration mechanisms. In this case, for electrons with a power-law injection spectrum, the slope does not change, while the spectrum itself is shifted toward higher energies. The coefficient K of the particle distribution function increases in accordance with the expression (Bogachev and Somov 2007)

$$K = K_0 \frac{\sqrt{1+(b_m-b)\,l^2}}{b\sqrt{b_m-b}} \times \int\limits_0^{\sqrt{1-b/b_m}} \left[\frac{1+x^2\left(bl^2-1\right)}{b}\right]^{-\gamma\varepsilon} dx, \quad (10)$$

where b and l are the transverse and longitudinal trap contraction parameters, respectively. At certain

Characteristics of the beam of accelerated electrons in the models with and without a reverse current

Model	$\gamma_{\mathbf{v}}$	$\gamma_{\mathcal{E}}$	γ_{SS}	n_b, cm^{-3}	F, erg cm^{-2} s^{-1}	$\varphi_{\rm cor}$	$\varphi_{\rm ch}$
Without reverse current	5.0	4.5	4.0	6.6×10^7	1.0×10^{10}	5.0 (4.6)	3.0 (3.0)
With reverse current	4.5	4.0	3.5	3.1×10^8	5.0×10^{10}	4.5 (4.6)	3.0 (3.0)

contraction parameters, the model spectrum of the coronal source closely coincides with the observed one (Fig. 3).

The results of our calculations of the hard X-ray spectra are presented in the table for the model of Syrovatskii and Shmeleva (1972) and our model. Recall that the slopes of the injection spectra are related between themselves as

$$\gamma_{SS} = \gamma_{\mathcal{E}} - 1/2 = \gamma_{\mathbf{v}} - 1,$$

where γ_{SS} is the slope of the energy spectrum for the flux of accelerated electrons, $\gamma_{\mathcal{E}}$ is the slope of the energy spectrum for the density of accelerated electrons. As has been noted above, we will describe the coronal and chromospheric sources in the form of thin and thick targets, respectively. If the reverse-current effect in the target model is disregarded, then this model will be called the classical one. The relations between the slope of the electron spectrum and the slope of the X-ray spectrum are known exactly for the classical model (see Somov and Syrovatskii 1976):

$$\varphi_{\rm cor} = \gamma_{SS} + 1 \quad \text{for thin target},$$
$$\varphi_{\rm ch} = \gamma_{SS} - 1 \quad \text{for thick target}.$$

It follows from the table and Fig. 3 that the electron spectrum in the thick-target model with a reverse current is harder than that in the classical model. For the same slope of the X-ray spectrum for the chromospheric source, both models give significantly different estimates of the spectral slope for the coronal source. Our model with a reverse current describes accurately the observational data both in the corona and in the chromosphere. The accuracy criterion here is that the estimates of the spectral slopes fall within the confidence intervals given in Krucker and Battaglia (2014). Meanwhile, the spectral slope in the corona estimated in the approximation of the classical model does not correspond to the observed picture.

4.2. Microwave Spectrum

Propagating with high velocities in a magnetic field, the accelerated electrons are known to produce bursts of microwave emission (in the nonrelativistic case, the so-called gyrosynchrotron emission). Particles with energies $\lesssim$100 keV form the part of the radio spectrum at low and medium frequencies, while the high-frequency part of the spectrum is entirely attributable to the emission of particles with energies $\sim$1 MeV or more. We calculated the radio spectrum for the July 19, 2012 flare separately for low- and high-energy particles (see Section 2) and then constructed the combined radio spectrum.

If the microwave source is assumed to be homogeneous, then the intensity observed near the Earth is defined by the solution of the corresponding transfer equation:

$$I_{MW} = I_{MW\perp} + I_{MW||} \qquad (11)$$
$$= \Sigma \frac{S_{MW}}{R^2} \frac{j_{\perp,||}}{\varkappa_{\perp,||}} \left[1 - \exp\left(-\varkappa_{\perp,||} l_0\right)\right],$$

where Σ is the sign of summation over the intensities of the emission components of the corresponding polarization, S_{MW} is the characteristic area of the source in the plane of the sky, $j_{\perp,||}$ and $\varkappa_{\perp,||}$ are the emission (absorption) coefficients for the perpendicular (parallel) polarization, respectively. We took the expressions for the emission and absorption coefficients from Fleishman and Kuznetsov (2010) and the computational algorithm from Ramaty (1969), Kuznetsov and Zharkova (2010), and Nita et al. (2015).

Figure 4 presents the radio spectrum calculated for $B_0 \approx 2 \times 10^2$ G. We can see a typical picture of gyrosynchrotron radio emission, where the bulk of the emission is generated by the high-energy electrons captured into a magnetic trap, against the background of the observed spectrum. Allowance for the reverse-current effect does not change the spectrum significantly (Kuznetsov and Zharkova 2010), because it barely affects the high-energy electrons. The model description of the spectrum may be considered satisfactory at high frequencies. The significant discrepancy between the results at low frequencies is probably related to the rough assumption about the homogeneity of the emission source and, as a consequence, to an overestimation of its density. Because of the Razin (1960a, 1960b) effect, which is more pronounced for a source with a high plasma density, the low frequencies are suppressed; therefore, the calculated intensity of the radio emission in this part of the model spectrum is well below the observed one.

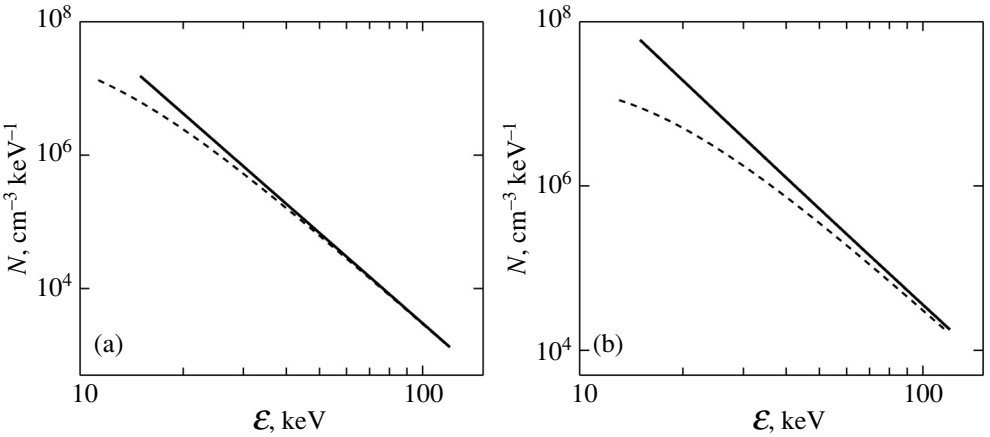

Fig. 5. Injection spectrum (solid straight line) and electron spectrum at depth $\xi = 3 \times 10^{19}$ cm^{-2} (dashed curve): (a) the classical thick-target model without a reverse current, (b) the thick-target model with a reverse current.

5. PLASMA HEATING BY ACCELERATED ELECTRONS

Krucker et al. (2015) considered three solar flares observed with high spatial and temporal resolutions, including the July 19, 2012 flare being considered here. A common feature of these flares is an anomalously high location of the hard X-ray and optical sources in the chromosphere. This fact cannot be explained in terms of the classical thick-target model (see also Krucker et al. 2011; Gritsyk and Somov 2014). To estimate the penetration depth of particles into the target and to understand the peculiarities of their propagation, let us calculate the energy spectra of accelerated electrons and the background plasma heating power.

In the previous section, based on the space observations of the July 19, 2012 flare, we found the reverse-current electric field strength (6) and the parameters of the injection spectrum (4) for each of the kinetic models. The energy spectrum of injected electrons as a function of depth ξ is defined by the expression

$$N(z,\xi) = \pi\left(\frac{2k_{\rm B}T_1}{m_e}\right)^{3/2}\int\limits_{-1}^{1} f_{\mathbf{v}}(z,\xi,\mu)\sqrt{z}d\mu. \quad (12)$$

The results of our calculations based on Eq. (12) for electrons with energies up to 120 keV in the July 19, 2012 flare are presented in Fig. 5. In the classical model (Fig. 5a), the injection spectrum has a slope $\gamma_{\mathcal{E}} \approx 4.5$ and the electron number density in the beam is $n_b \approx 6.6 \times 10^7$ cm^{-3}. In the thick-target model with a reverse current (Fig. 5b), the injection spectrum is harder, $\gamma_{\mathcal{E}} \approx 4.0$, at a number density $n_b \approx 3.1 \times 10^8$ cm^{-3}.

Let us calculate the power of the plasma heating in the target by accelerated electrons using the formula from Syrovatskii and Shmeleva (1972):

$$\mathcal{P}(\xi) = \frac{4\pi a_0}{{m_e}^2}(k_B T_1) \quad (13)$$
$$\times \int\limits_0^{\infty}\int\limits_{-1}^{1} f_{\mathbf{v}}(z,\xi,\mu)dzd\mu,\ \text{keV s}^{-1},$$

where the coefficient

$$a_0 = 2\pi e^4 \ln\Lambda$$
$$\approx 1.3 \times 10^{-19}\Big[\ln\left(\mathcal{E}/m_e c^2\right) - (1/2)$$
$$\times \ln n_2 + 38.7\Big],\ \text{keV}^2\,\text{cm}^2.$$

In the model with a reverse current, the pattern of plasma heating differs greatly from the results of our calculations for the classical model (Fig. 6). The main difference is that the electrons penetrate to smaller depths in the presence of a reverse current than they do in the classical model. Indeed, some beam electrons decelerate under the action of the reverse-current electric field, losing their kinetic energy, while others change the direction of their motion almost without energy losses. In addition, the electrons lose their energy through Coulomb collisions with plasma particles. Note that the plasma heating by reverse-current electrons (Sermulynsh and Somov 1983) was not estimated in the presented calculations. Meanwhile, allowance for the plasma heating by the reverse current will reinforce our conclusion about the absorption of beam energy in higher chromospheric layers (see Fig. 2.1.24 in Somov (1992)).

The results obtained describe the natural pattern of evolution of the spectrum of accelerated electrons and the plasma heating by them in the target. Note

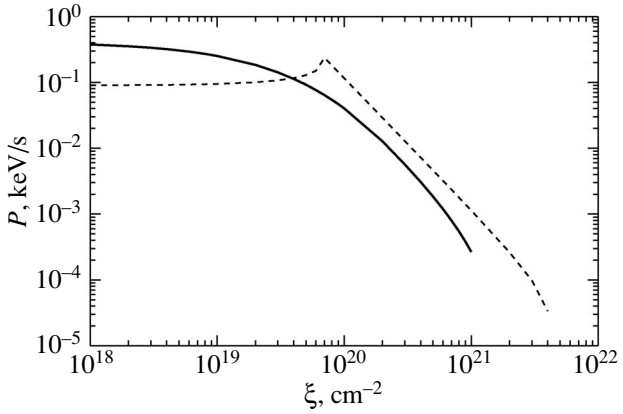

Fig. 6. Power of the plasma heating by accelerated electrons in the July 19, 2012 flare calculated in the thick-target model: without (dashed line) and with (solid line) a reverse current.

several significant peculiarities of the model with a reverse current.

First, to provide the required luminosity of the hard X-ray source in the chromosphere, it is necessary to deliver a sufficient number of fast electrons to certain depths. For this purpose, higher electron density in the beam and energy flux density, respectively, n_b and F in the table, than those in the model without a reverse current are needed in the model that takes into account the deceleration of fast electrons by the reverse-current electric field.

Second, a large number of beam electrons ($n_{bf} \approx 1.8 \times 10^7$ cm $^{-3}$) are turned around by the reverse-current electric field and move backward, toward the turbulent front TF. Such particles contribute to the intensity of the coronal hard X-ray source. Moreover, these fast electrons are on reconnected magnetic field lines, i.e., captured into a collapsing magnetic trap. Such particles provide additional coronal plasma heating to anomalously high temperatures, which can lead to a change in the parameters of the reconnecting current layer (Diakonov and Somov 1990).

Third, due to their considerably higher flux density, the accelerated electrons in the model with a reverse current carry a greater energy into the chromosphere, providing its more efficient heating. As a consequence, the hydrodynamic response of the chromosphere to impulsive heating by accelerated electrons (see Chapter 2 in Somov (1992)) must be stronger than that in the model with a reverse current, i.e., must have a larger amplitude at shorter times.

Using the December 6, 2006 solar flare as an example, we showed previously (Gritsyk and Somov 2014) that the reverse-current effect should be taken into account when modeling X-class flares. The reverse-current electric field strength in large flares is $\varepsilon > 1$, which determines the evolution of the distribution function (5) and, as a consequence, the characteristics of the observed emission. However, the field strength reaches $\varepsilon \sim 1$ even for such comparatively small flares as that considered here. In this flare, according to the estimates by Krucker et al. (2015), the chromospheric optical source is located anomalously high above the photosphere and, in addition, coincides in space and time with the chromospheric hard X-ray source.

In the thick-target model with a reverse current, it seems possible to describe the observed picture of the flare not only in the X-ray range but also in the optical one. Indeed, the accelerated electrons penetrate into the chromosphere to the optical flare depth, effectively losing their energy through Coulomb collisions and under the action of the reverse-current electric field. In other words, the electric field is mainly responsible for the high location of the chromospheric source, because it limits the flux of electrons into deep chromospheric layers. In this case, the flux density of the energy transferred by accelerated electrons into the chromosphere, which is almost an order of magnitude higher than that in the classical model, provides strong heating in the region where the optical and X-ray sources are located.

6. DISCUSSION AND CONCLUSIONS

Present-day spaceborne and ground-based observations of solar flares in various ranges of the electromagnetic spectrum with high temporal, spatial, and spectral resolutions provide an excellent basis not only for studying the individual physical processes in the flare but also for modeling the entire flare as a complex phenomenon in a plasma with strong

magnetic fields. Since the flares on the Sun are accompanied by the acceleration of a large number of charged particles carrying a significant fraction of the total flare energy, apart from the MHD processes, the kinetic ones also play a fundamental role in modeling them as a whole.

In this paper, we performed a kinetic modeling of the July 19, 2012 flare. We showed that the model without a reverse current did not allow the emissions from the coronal (in the thin-target approximation) and chromospheric (in the thick-target approximation) hard X-ray sources to be described simultaneously. Meanwhile, the observed relation between the spectral slopes in the solar corona and chromosphere $\varphi_{\rm cor} - \varphi_{\rm ch} < 2$ (see the table) is easy to interpret in terms of the thick-target model with a reverse current. Thus, the observation of two sources (in the corona and chromosphere) in one flare clearly demonstrates the necessity of taking into account the reverse-current electric field in constructing the kinetic flare model.

Note the second, no less important result obtained here. For the calculated spectrum of the coronal hard X-ray source, the slope closely coincides with the observed one (Fig. 3), but the radiation flux density is noticeably lower than the observed one. This contradiction suggests that an additional electron acceleration mechanism with a very peculiar property is required. The acceleration of particles in collapsing magnetic traps is such a mechanism (Somov and Kosugi 1997).

The original model with a reverse current (Section 3.1) disregards the acceleration of electrons that they acquire being captured into a collapsing magnetic trap. Meanwhile, fast electrons with any spectrum (including the Maxwellian one) acquire an additional kinetic energy in a collapsing magnetic trap through betatron heating and first-order Fermi acceleration (Somov and Bogachev 2003). In this case, for electrons with a power-law injection spectrum, the slope does not change, while the spectrum itself is shifted toward higher energies. Having applied the formula for the corresponding shift of the electron energy spectrum (Bogachev and Somov 2007), we made sure that the two-step particle acceleration predicted by Somov and Kosugi (1997) actually took place in the July 19, 2012 flare. This result (Section 3.2) is of special importance, because it points to the necessity of taking into account the additional acceleration of electrons in the trap when modeling solar flares. This is especially true for flares with a long impulsive phase, during which the configuration of the coronal trap changes dramatically.

The correctness of the model proposed here, primarily the validity of our calculated injection spectrum of accelerated electrons, can be judged by one more, observationally independent channel, the microwave emission. Our calculated spectrum at medium and high frequencies is consistent with the observational data from the NoRp instrument (Fig. 4). The low-frequency part of the spectrum is difficult to properly describe due to the absence of data on the plasma density distribution in the emission source (see Section 4.2).

We think that our results can also be used as the input ones for estimating the characteristics of the optical source, which will allow the model description of the flare to be made complete. However, the question about the formation of an optical continuum, i.e., a white-light flare, is beyond the scope of this paper, implying a detailed study of the hydrodynamic response of the chromosphere to impulsive heating by accelerated electrons under conditions when the energy losses through radiation cease to be optically transparent.

ACKNOWLEDGMENTS

We wish to thank the referees for their helpful remarks. This work was financially supported by the Russian Foundation for Basic Research (project nos. 14-02-31425-mol-a and 16-02-00585A).

REFERENCES

1. M. J. Aschwanden, *Particle Acceleration and Kinematics in Solar Flares* (Kluwer Academic, Dordrecht, 2002), p. 227.
2. S. A. Bogachev and B. V. Somov, Astron. Lett. **33**, 54 (2007).
3. A. Caspi, S. Krucker, and R. P. Lin, Astrophys. J. **781**, 43 (2014).
4. S. V. Diakonov and B. V. Somov, Solar Phys. **116**, 119 (1988).
5. S. V. Diakonov and B. V. Somov, Kinem. Fiz. Nebesn. Tel **6**, 48 (1990).
6. G. Elwert and E. Haug, Solar Phys. **15**, 234 (1970).
7. G. D. Fleishman and A. A. Kuznetsov, Astrophys. J. **721**, 1127 (2010).
8. R. G. Giovanelli, Mon. Not. R. Astron. Soc. **108**, 163 (1948).
9. P. A. Gritsyk and B. V. Somov, Moscow Univ. Phys. Bull. **66**, 466 (2011).
10. P. A. Gritsyk and B. V. Somov, Astron. Lett. **40**, 499 (2014).
11. S. S. Holt and R. Ramaty, Solar Phys. **8**, 119 (1969).
12. H. Hudson and J. Ryan, Astrophys. J. **33**, 239 (1995).
13. S. Krucker and M. Battaglia, Astrophys. J. **780**, 107 (2014).
14. S. Krucker, H. S. Hudson, N. L. S. Jeffrey, M. Battaglia, E. P. Kontar, A. O. Benz, A. Csillaghy, and R. P. Lin, Astrophys. J. **739**, 96 (2011).

15. S. Krucker, P. Saint-Hilaire, H. S. Hudson, M. Haberreiter, J. C. Martinez-Oliveros, M. D. Fivian, G. Hurford, L. Kleint, M. Battaglia, M. Kuhar, and N. G. Arnold, Astrophys. J. **802**, 19 (2015).
16. A. A. Kuznetsov and V. V. Zharkova, Astrophys. J. **722**, 1577 (2010).
17. J. Leach and V. Petrosian, Astrophys. J. **251**, 781 (1981).
18. J. R. Lemen, A. M. Title, D. J. Akin, P. F. Boerner, C. Chou, J. F. Drake, D. W. Duncan, C. G. Edwards, et al., Solar Phys. **275**, 17 (2012).
19. R. P. Lin, B. R. Dennis, G. J. Hurford, D. M. Smith, A. Zehnder, P. R. Harvey, D. W. Curtis, D. Pankow, et al., Solar Phys. **210**, 3 (2002).
20. Yu. E. Litvinenko and B. V. Somov, Solar Phys. **131**, 319 (1991).
21. R. Liu, Mon. Not. R. Astron. Soc. **434**, 1309 (2013).
22. W. Liu, O. Chen, and V. Petrosian, Astrophys. J. **767**, 168 (2013).
23. L. I. Miroshnichenko, *Solar Cosmic Rays, Fundamentals, and Applications,* 2nd ed. (Springer, Heidelberg, 2015).
24. G. M. Nita, G. D. Fleishman, A. A. Kuznetsov, E. P. Kontar, and D. E. Gary, Astrophys. J. **799**, 236 (2015).
25. L. Nocera, Yu. I. Skrynnikov, and B. V. Somov, Solar Phys. **97**, 81 (1985).
26. G. H. J. van den Oord, Astron. Astrophys. **234**, 496 (1990).
27. E. N. Parker, J. Geophys. Res. **62**, 509 (1957)
28. E. R. Priest and T. Forbes, *Magnetic Reconnection: MHD Theory and Applications* (Cambridge Univ. Press, Cambridge, UK, 2000).
29. R. Ramaty, Astrophys. J. **158**, 753 (1969).
30. V. A. Razin, Izv. Vyssh. Uchebn. Zaved., Radiofiz. **3**, 584 (1960a).
31. V. A. Razin, Izv. Vyssh. Uchebn. Zaved., Radiofiz. **3**, 921 (1960b).
32. V. Sermulynsh and B. V. Somov, Issled. Solntsa Krasn. Zvezd **18**, 86 (1983).
33. B. V. Somov, *Physical Processes in Solar Flares* (Dordrecht, London, 1992).
34. B. V. Somov, *Cosmic Plasma Physics* (Kluwer Academic, Dordrecht, 2000).
35. B. V. Somov, *Plasma Astrophysics*, Ch. I: *Fundamentals and Practice* (Springer SBM, New York, 2012).
36. B. V. Somov, *Plasma Astrophysics*, Ch. II: *Reconnection and Flares* (Springer SBM, New York, 2013), p. 504.
37. B. V. Somov and S. A. Bogachev, Astron. Lett. **29**, 621 (2003).
38. B. V. Somov and T. Kosugi, Astrophys. J. **485**, 859 (1997).
39. B. V. Somov and S. I. Syrovatskii, Sov. Phys. Usp. **19**, 217 (1976).
40. P. A. Sweet, Nuovo Cimento Suppl. **8**, Ser. 10, 188 (1958).
41. P. A. Sweet, Ann. Rev. Astron. Astrophys. **7**, 149 (1969).
42. S. I. Syrovatskii, Sov. Astron. **6**, 768 (1962).
43. S. I. Syrovatskii, Sov. Astron. **10**, 270 (1966).
44. S. I. Syrovatskii and O. P. Shmeleva, Sov. Astron. **16**, 273 (1972).
45. S. I. Syrovatskii and O. P. Shmeleva, in *Solar Terrestrial Relations,* Ed. by D. Venkatesan (Univ. Calgary, Canada, 1973), p. 243.

Translated by V. Astakhov